The Lunar Orbiter Laser Altimeter Investigation on the Lunar Reconnaissance Orbiter Mission

David E. Smith[1], Maria T. Zuber[2], Glenn B. Jackson[3], Haris Riris[1], Gregory A. Neumann[1], Xiaoli Sun[1], Jan F. McGarry[1], John F. Cavanaugh[3], Luis A. Ramos-Izquierdo[3], Ronald Zellar[3], Mark H. Torrence[4], Erwan Mazarico[1], Joseph Connelly[3], Adam Matuszeski[3], Melanie Ott[3], David D. Rowlands[1], Thomas Zagwodzki[2], Mark H. Torrence[4], Rich Katz[3], Igor Kleyner[3], Carlton Peters[3], Peter Liiva[5], Craig Coltharp[3], Stephen Schmidt[3], Lawrence Ramsey[3], Vibrart S. Scott[3], Glenn Unger[3], Danny C. Krebs[3], Anne-Marie D. Novo-Gradac[3, 6], George B. Shaw[3], and Anthony W. Yu[3]

[1]Solar System Exploration Division, NASA Goddard Space Flight Center, Greenbelt, MD 20771, USA.
[2]Department of Earth, Atmospheric and Planetary Sciences, Massachusetts Institute of Technology, Cambridge, MA 02139-4307, USA.
[3]Advanced Engineering Technology Directorate, NASA Goddard Space Flight Center, Greenbelt, MD 20771, USA.
[4]Stinger Ghaffarian Technologies, Greenbelt, MD 20770, USA.
[5]Sigma Space Corporation, Lanham, MD 20706
[6]Now at: Astrophysics Division, NASA Headquarters, Washington, DC 20546

Submitted to:
Space Science Reviews
January 5, 2008

Abstract

The Lunar Orbiter Laser Altimeter is an instrument on the payload of NASA's Lunar Reconnaissance Orbiter spacecraft (Chin et al., 2007). The instrument is designed to measure the shape of the Moon by measuring precisely the range from the spacecraft to the lunar surface, and incorporating precision orbit determination of LRO, referencing surface ranges to the Moon's center of mass. LOLA has 5 beams and operates at 28 Hz, with a nominal accuracy of 10 cm. Its primary objective is to produce a global geodetic grid for the Moon to which all other observations can be geodetically referenced.

Keywords Moon, shape, space instrumentation, topography

1. Introduction

The Lunar Orbiter Laser Altimeter (LOLA) is an instrument designed to assist in the selection of landing sites on the Moon for future robotic and human exploration. The primary motivation is that any future mission that proposed to land on the surface of the Moon would need to be sure from the best available information that the location would be safe for both robotic and human endeavors. In this context, LOLA was proposed to the payload of the Lunar Reconnaissance Orbiter (LRO) mission (Chin et al., 2007) to provide the geodetic location, the direction and magnitude of surface slopes, and the variation in elevation in the region, the latter generally referred to as surface roughness. In addition, since one of the objectives of NASA's Exploration Program was to attempt to detect the presence of water ice on or near the surface, LOLA was designed to measure the reflectance of the surface at the laser wavelength such that any significant water ice crystals on the lunar surface would provide a measurable increase in reflectance.

The present knowledge of the topography of the Moon (cf. (Wieczorek, 2007) is not adequate for ensuring a safe landing in any but a few locations, such as those visited by the Apollo flights. Based upon all previous missions to the Moon, knowledge of the position of features on the surface is at approximately the kilometer level and in many areas, such as the lunar far side, that knowledge is of order many kilometers. In addition, the slope of the surface at the majority of locations is completely unknown on scales of 10's to 100's of kilometers. For topography, and more generally for the shape of the Moon, the major source of data has been the Clementine mission (Nozette et al., 1994), launched in 1994, which carried a laser altimeter that provided the first near-global mapping of the Moon (Zuber *et al.*, 1994; Smith *et al.*, 1997); the exception being the regions within about 10 to fifteen degrees of each pole. The data are estimated to have provided 100-m quality radial information and similar horizontal quality position information with a spatial resolution of order 1 degree (~30 km) at the equator. The lunar shape measured by Clementine is shown in Fig. 1 (Zuber et al., 1994). A more recent effort combined Clementine altimetry (Smith et al., 1997) with elevation models of the lunar polar regions from stereo-photogrammetry (e.g. (Cook *et al.*, 2000). This model (Survey, 2002) has improved spatial resolution at the poles but lacks geodetic control.

Recently, laser altimeters have flown to the Moon on missions from the Chinese, Japanese and Indian space agencies. The Chinese (Qian, 2008) and Japanese (Araki et al., 2007) instruments, both single-beam 1-Hz ranging systems, operated successfully but these data sets have not yet been generally released. The Indian instrument (Kamalakar et al., 2005), a single-beam 10-Hz ranging system similar to MOLA at Mars (Zuber *et al.*, 1992; Smith *et al.*, 1999), has not yet begun mapping. While all of these instruments likely will or are expected to provide possibly considerable improvements in lunar topographic knowledge, none of them have performance specifications that meet the requirements delineated by the NASA Exploration Program.

In order to improve significantly our knowledge of the lunar topography it was necessary employ a greater accuracy altimetric ranging system and be able to determine the position of the LRO spacecraft to significantly greater accuracy than had been achieved on earlier missions. In addition, the spacecraft altitude and the timing of the observations would be needed to commensurate accuracy.

2. Investigation Description

2.1 Exploration

The LOLA investigation is designed to assist in the selection of future landing sites by providing topographic, surface roughness, surface slope, and surface reflectance measurements, and a global lunar coordinate system that provides information on the positions of lunar surface features. In the design and development of the instrument certain assumptions were made about the geodetic requirements for landing on the lunar surface, particularly spatial resolution and positional accuracy. The assumptions that we used to guide the instrument performance are shown in Table 1. These assumptions are in 3 categories: landing site knowledge, instrument performance, and spacecraft positional and orbital knowledge.

In order for positional accuracies to be achieved globally, it is necessary to develop an improved lunar reference system or grid that has an internal consistency at the ~50-m level. This grid could then be compared with the known positions of the Apollo landing sites so that all LRO and previous lunar data could be incorporated into the LRO/LOLA-derived coordinate frame. The development of an accurate (~50-m) global geodetic grid was considered to be the highest priority objective of the LOLA investigation that would ultimately provide the control at regional and local scales. An internal consistency at the 50-m level also requires spatial positioning of the LRO spacecraft of similar quality, which in itself requires improvements be made to the lunar gravity model. This improvement is expected to come from the global coverage of laser altimeter data in combination with tracking of the LRO spacecraft. Nominal LRO tracking is by the Universal Space Network (USN) at S-band with approximately ±1 mm/s Doppler per 10 s augmented by laser ranging (LR) (Zuber *et al.*, 2008b), which is able to provide approximately ±10 cm range measurements at 28 Hz.

The determination of the full surface slope requires the measurement of slope in two directions and hence the altimeter must make measurements across track as well as along track. This requirement is accomplished in LOLA by a multi-beam approach that provides 5 measurements in an X-pattern from which the slopes along track and across track can be derived. This X-formation also has the advantage that, suitably rotated, will provide, 5 near-equidistant parallel profiles, in LOLA's case with approximately 12 m between profiles. Fig. 2 shows the 5-spot pattern on the lunar surface that LOLA will implement.

The 5 parallel profiles, providing 5 measures of altitude, surface roughness, and surface brightness, for each laser pulse, characterize a continuous strip of the lunar surface 50- to 60-m wide and will provide an assessment of the suitability of the area as a "lunar landing strip". Graphical displays of the data from LOLA, provided within hours of the data being returned will show the elevation of the surface, an estimate of the surface roughness and surface reflectance, and the derived measurements of the slope of the surface. Fig. 3 shows the large number of slopes on various baselines derivable from 10 observations obtainable in less than 0.1 seconds of operation.

The surface reflectance represents a measure of the albedo of the surface at the laser wavelength of 1064 nm and has been designed into the instrument with the aim of being able to detect the presence of surface ice at small areal density. The measurement is accomplished by estimating the energy of the return laser signal and comparing it with the output energy. Note that this measurement is calibrated in a relative sense, with respect to pre-launch testing, as the instrument lacks a source with known brightness in flight. Nonetheless, experience has shown the measurement to be extremely stable based on experience in ranging at Mars (Smith et al., 2001; Sun et al., 2001). The brightness of ice crystals on the lunar surface is expected to have an albedo that is approximately 4 times the albedo of the regolith. Thus an albedo measurement of 10 to 15% in each of the spots would enable ice crystal densities of 4 or 5% on the lunar surface to be detected. The possible detection of surface ice by LOLA, although not the instrument's prime measurement, is considered a potential high-priority opportunity to address one of LRO's mission objectives.

The altimeter operates continuously providing 5-spot data in a 50- to 60-m swath along the track of the spacecraft. The resolution across track depends on the number of orbits of the spacecraft. After 1 year the across-track resolution is approximately 0.04^{o}, providing an average separation of the LOLA swaths at the equator of order 1.2 km, and at latitudes 80N&S a separation of order 200 m. Fig. 4a and 4b show the coverage from 88S to the pole for a typical month and 80S to the pole; each month is very similar to the next although the ground tracks do not repeat.

2.2 Science

In addition to providing measurements for exploration the LOLA Investigation Team will also conduct a variety of scientific studies to address a wide variety of outstanding questions in lunar science.

(a) LOLA will improve the current understanding of impact flux on the Moon, especially during its early history, by helping identify and characterize topographic expressions of crater-like circular structures (Frey et al., 2002) and their size-frequency distribution, thus providing new constraints on the cratering history subsequent to the late heavy bombardment. In addition, LOLA will provide greater insights on the factors that contribute to the formation of craters, including improvements to the connection between an observed crater and the projectile size / impact velocity which generated it, yielding an improved understanding of the size-frequency distribution of the primary impactor population striking the Moon.

(b) Topography and gravity are fundamental measurements that provide information on the lunar interior structure. LOLA topography in combination with high-resolution gravity soon to be available from the Gravity Recovery and Interior Laboratory (GRAIL) mission (Zuber et al., 2008a) will be used to map the Moon's global crustal and lithosphere thickness as well as crustal and mantle density anomalies. These observations will be applied to study the structure of impact basins as a measure of the influence of impactors on the shallow interior of the Moon.

Models of the planet interior depend explicitly on the estimate of the polar moment of inertia, which measures the radial distribution of mass. The k_2 Love number of the Moon, which measures the tidal response of the potential, has been determined from analysis of satellite tracking data (*e.g.* (Konopliv *et al.*, 2001), k_2=0.026 ± 0.003; (Goossens and Matsumoto, 2008), from a re-analysis of LP and historical data found 0.0213 ± 0.0075). The LRO data will lead to an independent (re-estimate) of this important physical parameter. In addition, from altimetry and LRO laser ranging (LR) (Zuber *et al.*, 2008b) we will be able to estimate the global h_2 Love number – which reflects the global geometric radial response of the Moon to tidal deformation and whose uncertainty is currently ~25%.

(c) Lunar albedo measurements, independent of illumination conditions, can be made by LOLA. To characterize possible volatiles in permanently shadowed polar regions, LOLA provides a bidirectional reflectance (albedo) at zero phase angle by means of the ratio of transmitted and returned energy measurements, and be capable of revealing concentrations of a few percent of surface water ice.

(d) LOLA data will be used to make quantitative assessments of volcanic landforms and source regions, and the characterization of lava flows and their stratigraphic relationships. Magmatic intrusions (dikes and sills) result in unique patterns of uplift and deformation at the surface that can be used to invert for the geometry of the underlying magma bodies. LOLA topographic data will be used to discriminate between magmatic and non-magmatic tectonism, and to constrain the volumes of the underlying magma bodies. Similar analyses have been successfully applied to the study of dikes on the Earth and Mars (e.g. (Schultz *et al.*, 2004)).

(e) LOLA data will be used to improve knowledge impact cratering and the processes in shaping planetary crusts, particularly in early history. New information will be obtained at all scales including multi-ring basins that play a significant role in shaping the topography of the terrestrial planets. The topographic signature of basin ring structures on the Moon is presently poorly resolved in Clementine topography. LOLA topography will enable the first high-resolution study of well-preserved multi-ring structures, thereby providing important information regarding their underlying structure and formation.

(f) Ejecta generated by impact processes constitute one of the primary sources of regolith and influences its subsequent evolution. High-resolution topographic analyses of ejecta at lunar craters using LOLA will provide new constraints on the thickness, run out, roughness, and block-size distributions of such ejecta as a function of crater and basin size. These measurements collectively provide a quantitative means to assess the role of ejecta in the formation and evolution of regolith.

In addition, many science objectives are enabled or supported by the knowledge of topography, roughness, and surface slopes, and precision laser tracking and orbit determination of LRO. Thus, LOLA will re-analyze its data using the GRAIL gravity model that is expected in 2012 and thereby improve geodetic framework for all other lunar data. Also, we plan to combine the Kaguya (Araki et al., 2007) and Chandrayaan (Kamalakar et al., 2005) altimetry with LRO data for an extended, fully compatible and inter-calibrated dataset and combine LOLA and LROC data, in a joint LOLA/LROC activity, for geodetically-controlled stereo topography to obtain the highest-resolution DEMs. The LOLA global data products, working with LROC (Robinson et al., 2008), will be cartographically-tied to the Lunar Laser Retro Reflectors (Dickey et al., 1994) and the Apollo and Lunakhod sites and thus incorporate the most precise lunar orientation / libration properties.

2.3 Orbit Determination for LOLA

The quality of the topographic measurements and models depends upon the quality of the altimeter and its supporting data, and also on the accuracy of the spacecraft orbit. The routine operational tracking data of LRO will be S-band Doppler acquired for approximately 20 hours per day and an accuracy of order 1 mm/s every 10 seconds. The altimeter has decimeter accuracy but the orbital error is expected to be significantly larger. Orbits for LRO will be developed by the LOLA team using a combinations of the S-band Doppler and laser tracking (Zuber *et al.*, 2008b) in conjunction with the altimetry. An important tool of the LOLA orbit determination activity is the altimeter used in the orbital crossover mode. At an orbital crossover the lunar radius is the same, as is the surface roughness, and the implied surface slopes. The equivalence of these measurements at the same location on different orbits enables the location of the crossover to be determined and the altimeter measurements used as an observable in determining the orbit of LRO, and also for estimating other parameters, such as pointing and timing, and gravity coefficients of the lunar gravity field (Rowlands et al., 1999). In addition, the very precise laser ranging (LR) observations (Zuber *et al.*, 2008b) will constrain the LRO orbit to the decimeter level over the lunar near side and will

significantly improve the orbit accuracy beyond that which will be achievable with S-band Doppler tracking alone, and further enable the estimation of additional force model parameters. At the conclusion of the analysis of all the LOLA data and the simultaneous LRO orbit determination we expect the global radial positional accuracy at the 50-cm level and at the 25-m level in the horizontal. Further details on the crossover analysis are given in Section 6.

3. Instrument Design

3.1 Overview

The Lunar Orbiter Laser Altimeter (LOLA) is one of the six science instruments and a technology demonstration on the LRO Mission (Chin et al., 2007). LOLA uses short pulses from a single laser through a Diffractive Optical Element (DOE) to produce a five-beam pattern that illuminates the lunar surface (Fig 2). For each beam, LOLA measures the time of flight (range), pulse spreading (surface roughness), and transmit/return energy (surface reflectance). The LOLA measurements will be used to produce the high-resolution global topographic model and global geodetic framework described in the previous section to enable the precise targeting, landing to carry out exploration activities. In addition, it will characterize the polar illumination environment, and image permanently shadowed regions of the lunar surface to identify possible locations of surface ice crystals in shadowed polar craters. The following sections describe the instrument design, pre-launch testing, and calibration results based on the pre-launch test data.

The LOLA instrument configuration is shown in Fig. 5 and the key instrument parameters are shown in Table 2. LOLA uses a Q-switched Nd:YAG laser at 1064 nm and avalanche photo diodes (APD) to measure the time of flight (TOF) to the lunar surface from a nominal 50-km orbit. The transmitted laser beam is split in five different beams by a diffractive optical element (DOE) with 0.5-mrad spacing. The receiver telescope focuses the reflected beams into a fiber optic array, placed at the focal plane of the telescope. The array consists of five fibers and each fiber in the array is aligned with a laser spot on the ground. The fibers direct the reflected beams into five detectors. The detector electronics amplify the signal and time stamp the received pulses relative to the spacecraft mission elapsed time (MET) using a set of time-to-digital converters (TDC) with 0.5-ns resolution. The transmitted pulse is also time stamped and the TOF to the lunar surface can be determined. The LRO spacecraft carries an ultra-stable quartz oscillator and distributes the timing signal to LOLA and other instruments. A signal-processing algorithm running on an embedded processor continually adjusts the receiver gain and threshold levels and maintains the range window centered on the lunar surface return. A functional block diagram of LOLA is shown in Fig. 6.

The LRO spacecraft also carries a unique laser ranging (LR) system (Zuber *et al.*, 2008b) for precise orbit determination. The laser ranging system consists of a 30-mm aperture optical receiver mounted on the LRO spacecraft high gain antenna used for

communications and data transmitting. The receiver is pointed to a ground (Earth) based laser satellite ranging station that sends a 532-nm laser pulse to LRO. The receiver focuses the incoming 532-nm beam into a fiber bundle and the laser pulses are then directed onto one of the five LOLA detectors modified to accommodate both 532 and 1064 signals. The LR system is described in a companion paper (Zuber *et al.*, 2008b).

3.2 LOLA Transmitter

The LOLA transmitter consists of two virtually identical, diode pumped, Q-switched Nd:YAG oscillators operating at 1064.4 nm (Fig. 7). The diode pump lasers are derated to increase their lifetime. The laser beams are combined with polarizing optics and only one laser is operating at a time; the other one is redundant. The laser repetition rate is 28 ± 0.1 Hz, the energy per pulse is ~ 2.7 mJ for Laser 1 and ~ 3.0 mJ for Laser 2. The pulse width is approximately 5 ns. The output of the laser is directed through an ×18 beam expander and then through a diffractive optical element that produces five beams separated by 500 ± 20 μrad. The laser beam prior to the beam expander has a divergence of 1.8 mrad. After the beam expander and the diffractive optical element, each beam has a 100 ± 10 μrad divergence and approximately the same energy; some variation in the energy between beams is discernible due to imperfections in the diffractive optical element. The LOLA laser is designed to operate in vacuum but a significant amount of the subsystem and system testing was done in air. The laser cavity was integrated in a clean room and two filters in the laser housing are designed to prevent particulate and molecular contamination of the laser topics prior to launch.

The laser beam pattern is clocked at 26^{o} relative to the spacecraft velocity vector. From the nominal orbit of 50 km, each laser spot is ~5 m in diameter on the ground. The five-spot pattern will allow LOLA to measure both the slope and roughness of the lunar surface. The five beam spot pattern on the ground (including the field of view) relative to the spacecraft velocity vector is shown in Fig. 2.

A small kick-off mirror placed inside the laser box directs a small fraction of the laser power onto a silicon segmented photodiode (SPOT-4) detector. The detector monitors the energy of the transmitted laser pulse and it also used as a fire acquisition signal that turns off the drive to the pump diode lasers. In addition, the outgoing pulse is time tagged and provides timing information for the time of flight measurement.

Pulse width. LOLA monitors the laser-pulse energy and the pulse width at threshold crossing, which may be used to infer the transmitted laser-pulse shape. Note that the pulse shape output from the LOLA SPOT 4 detector is the convolution of the actual pulse shape and the impulse response of the transmit energy monitor. (The nominal rise time for the SPOT 4 detector is 3 ns but in testing with the breadboard laser to determine its characteristics a tail was observed). The relationship between the LOLA measured pulse width and the threshold value for Laser 1 and 2 was measured and the result is given in Fig. 10. The nominal transmit threshold setting is 116 mV. The average transmitted laser pulse energy is not expected to decrease significantly over the mission lifetime, thus the threshold value for the transmitted pulse should not have to be adjusted. If the laser

or the transmitter common optics were to degrade, the threshold could be lowered to continue detecting transmitted laser pulses. There is approximately a factor of six adjustment that can be made on the transmit threshold (from 116 to 19 mV).

Life Testing of Transmitter. As part of the development of the transmitter a parallel life test program was conducted in order to verify the basic design, identify areas requiring modification, and provide an estimate of the lifetime that can be expected on orbit. This was particularly important for LOLA because of the use of a double transmitter system that would was expected to enable extended life of the instrument. The goal of the instrument was to acquire 1 billion pulses from each laser thus providing approximately 5 billion altimetric, pulse spreading and surface albedo measurements.

Three life tests at various stages were conducted. The first was on an early design that operated continuously for approximately 560 million shots that verified the basic design. The second test on a pre-engineering model (pre-EM) of the Laser 1 operated for approximately 520 million shots, and test 3 (presently in process) on an EM of Laser 2, has lasted accumulated over 220 million shots without degradation. The requirement of the LRO mission for exploration is approximately 880 million total shots.

3.3 LOLA Receiver and Detector

The LOLA receiver consists of a 14-cm-diameter clear aperture refractive telescope with that focuses the received photons on to a fiber optic bundle (FOB). The effective focal length of the telescope is 500 mm. The design and materials of the telescope were chosen to minimize the thermal fluctuations expected on orbit. Since LOLA is not an imaging system, the concern is not to maintain the image quality but to collect the maximum number of photons with the fewest possible losses and to minimize the background radiation. The telescope assembly includes a dielectric fold mirror, which lets all radiation other than 1064 nm pass through and reflects the laser radiation onto the FOB. This minimizes the amount of background solar radiation incident on the detectors. The fiber bundle consists of five identical fibers. Each fiber in the bundle directs the reflected energy into the aft-optics assembly for each detector. The receiver and fiber bundle are shown in Fig. 8.

The aft optics assemblies for detectors (channels) 2-5 are identical (Fig. 9). Detector 1 houses the laser LR aft optics. The aft-optics assembly mounts directly on a flange that is an integral part of the detector housing assembly. The housing assembly or detector plate includes the detector and all the associated electronics. The aft optics consists of collimating and focusing optics to collimate the output of the fiber and send it on to the detector. A bandpass filter tuned to the laser wavelength is also included in the optical train to minimize the background solar radiation. In addition, the aft optics assembly includes a separate test port with an FC connector. The test port is intended for calibration purposes during instrument integration and testing. Signals from optical test sources can be injected into the test port and exercise the signal processing algorithms and electronics of the instrument. It is also possible to back-illuminate the detectors

through the test port and monitor the field of view (FOV) and boresight alignment during the integration process.

The LOLA detectors are part of the detector housing assembly. The housing assembly includes the aft optics, the detector hybrid and the LOLA detector board. The detectors and detector board electronics have low noise and sufficient bandwidth to allow detection of the reflected laser pulses from the lunar surface and measure the time of flight (TOF). Each detector has its own independent gain control and threshold setting. The detector hybrids are the same silicon avalanche photodiodes that were used on the Mars Orbiter Laser Altimeter (MOLA) (Zuber et al., 1992) and the Geoscience Laser Altimeter (GLAS) (Schutz, 2001; Abshire *et al.*, 2005).

The LOLA detector board amplifies the detector hybrid output, and performs two separate functions: a discrimination function to provide timing information to the Digital Unit (DU), and an energy measurement function that integrates and samples the peak of the amplified hybrid output.

The amplification of the hybrid output is performed by a variable gain amplifier (VGA) and a fixed gain buffer with a gain of 5. The VGA gain is variable over a range of <0.5 to 10, controlled by an externally generated d.c. voltage from the DU. The gain control voltage is scaled and level-shifted on the detector board. The discrimination function for the timing information is performed by a high-speed comparator. The threshold level is set by the DU and fed directly to the comparator input.

The energy measurement function is performed by an integrator and a peak detector. It is not dependent on the threshold set by the DU but it is affected by the gain setting. The integrator stage is combined with a track-and-hold function, which is controlled by a latch. The latch is set by a peak detector, and later reset by a signal from the DU. The peak detector responds to the integrator output so as to set the latch at the time of the maximum output from the integrator. The latch then puts the integrator into its HOLD mode until its output is digitized. The peak detector is an a.c.-coupled, d.c. offset constant-fraction discriminator. The output is proportional to the received energy.

3.4 ***LOLA Digital Unit***

The LOLA Digital Unit provides two fundamental categories of functionality for the instrument. The first category - range measurement - includes firing the laser and acquiring Earth and LR data. The other category – command and telemetry (C&T) - comprises receiving and distributing spacecraft commands, collecting, formatting and transmitting telemetry, as well as monitoring and processing ranging information for real-time control of the altimeter's parameters such as the range gate, amplifier gain and detector threshold.

Two different time measurements are made by the electronics. The primary is the time-stamping of the laser transmit pulse and the five lunar return pulses, and the LR pulse. The timing reference is based on redundant 20 MHz ultra stable oscillators (USO) located

in the spacecraft, which is divided to 5 MHz and used as the internal timing reference. The spacecraft provides a non-redundant 1 Hz pulse, which is used to synchronize all LOLA activities. The fault-tolerant design allows for the spacecraft timing signals to replace the function of the internal clock oscillator, while the internal oscillator is sufficient to operate the instrument in the absence of any spacecraft timing reference. Also, circuits will use the spacecraft's USO to measure the frequency of the oscillator, for purposes of calibration and trending.

LOLA operates at a pulse repetition rate (PRF) of 28 Hz phase locked to the spacecraft's 1-Hz timing signal. Each 1 s interval is referred to as a major frame, which consists of 28 approximately 35.7 ms periods referred to as a minor frames. The time within a minor frame is allocated for various functions, which include an 8 ms window for receiving the Earth laser signal (LR), a window for receiving the reflections from the Moon, and time for transmitting science and engineering data to the Command and Telemetry Electronics. The Range Measurement Electronics also synchronizes the operation of the Analog Electronics and controls resetting of the energy measurement circuits for Detector boards. The Range Measurement Electronics control is implemented in a single RTAX2000S Field Programmable Gate Array (FPGA). This FPGA also contains a variety of counters which implement the 200-ns coarse timer for each channel, noise counters, event counters, and calibration counters for measuring the margin in the digital phase lock loops in each of the twelve fine timing microcircuits. There are six physical channels in the Range Measurement Electronics. One channel is utilized for the timing laser firing pulse, and the other five are for the lunar return pulses, with one of the return channels also time-shared for the Earth laser time measurement. The time measurement method utilizes a coarse timer implemented in the FPGA along with fine timing supplied by the digital ASIC time-to-digital converter (TDC) originally designed to support the ESA's Automated Transfer Vehicle (ATD). The FPGA and TDC circuits together allow for time-tagging over planetary distances of the time that the laser is fired, the time the Earth-based laser's signal (LR) arrives at the spacecraft, and the time of each of 5 returns are received from the Moon; the LOLA altimeter has a resolution of approximately 28 ps.

3.5 Laser Transmitter Telescope

The LOLA laser transmitter telescope has two functions: it reduces the divergence of the LOLA laser oscillator input beam, and it splits the output beam into five to generate a cross pattern in the far field. The telescope is an 18X magnification, afocal, Galilean beam expander that expands and collimates the LOLA Laser 1mm and 1.8 mrad $1/e^2$ diameter input beam to generate the required 100μrad $1/e^2$ diameter output beam divergence. The telescope has a single Corning 7980 fused silica negative lens, a BK7G18 positive lens group, and a diffractive beam splitter (DOE) that generates five output beams from a single input beam. The DOE optic is a 40-mm diameter by 6-mm thick fused silica substrate etched on one side with a transmission phase grating and anti-reflection (AR) coated on both sides to maximize transmission at 1064 nm. The LOLA DOE was manufactured by MEMS Optical from a master pattern that is replicated via a proprietary lithographic process onto a fused silica wafer from which multiple parts can

be cored out. The flight DOE had an overall efficiency of 80% with the center beam having nearly twice the energy of the outer beams.

The telescope tube is beryllium with a titanium flexure pre-loaded to 30 lbs in order to securely hold the positive lenses and DOE over all expected mechanical and thermal loads. The exit optics contain a 36-mm diameter exit clear aperture. The LOLA assembly is 165 mm long and weighs 120 g, has an operational thermal range of 20 ± 20 C, and a survival thermal range of -30 C to +70 C. Two flight model (FM) Laser Transmitter Telescopes were integrated, functionally tested in air and vacuum, thermally qualified for survival, and delivered to the LOLA laser team for integration to the Laser Bench. Further details on the transmitter telescope are given in (Ramos-Izquierdo and al., 2009).

3.5 LOLA Receiver Telescope

The LOLA Receiver Telescope (LRT) has a 150-mm diameter objective lens and an unfolded path length to provide an *f/2* objective lens speed. The LOLA Receiver Telescope opto-mechanical design is a beryllium structure with titanium flexures, tolerances, optic mounting techniques, and alignment compensators for focus and boresight. The receiver FOV is determined by the FOB located at the telescope focal plane. The telescope end of the FOB has five 200-μm core diameter, 0.22 NA, multimode, step-index fiber-optics spaced 250 μm apart in a cross pattern; these fiber-optics define five 400-μrad diameter FOV's with a center-to-center spacing of 500 μrad. The FOB telescope connector is clocked 26^{o} to align the five receiver FOV's with the five transmitted laser beams. Behind the telescope connector the FOB fans out into five independent fiber-optic cables that attach to the five Aft-Optics/Detector Assemblies. The LOLA receiver system FOV was selected to provide sufficient boresight alignment margin for each laser/receiver pair while having enough angular distance between neighboring channels to prevent crosstalk. Further details regarding the LRT are given in (Ramos-Izquierdo and al., 2009).

4. System Calibration

4.1 Transmitter Energy Calibration

The LOLA transmitter has an on-board laser energy sensor (detector), which also serves as the fire acquisition detector. The detector is commonly referred as the SPOT4 or Transmit energy (*Tx* Energy) monitor. The transmit energy monitor was correlated with measurements made with an external energy meter to assess its performance at the system level (Fig. 11).

By correlating and normalizing the *Tx* Energy monitor with the external energy monitor it is possible to measure the transmitted energy with approximately 1.3 % accuracy. There was no degradation in the accuracy performance of the *Tx* Energy monitor as a function of temperature. Using data for Laser 1 in the hot and cold plateaus we determined that in the hot case the accuracy was 0.5%-1% and in the cold case it was approximately 1.0%.

Thus, we can expect the *Tx* energy accuracy requirement of 2% to be met at all temperatures.

The equation that converts *Tx* Energy monitor from counts to laser energy is given below:

$$Energy\ (mJoules) \approx\ 2.0 \times 10^{-2}\ \times\ Tx\ Energy\ (counts) -\ 0.24 \qquad (1)$$

The equation was obtained using ambient data (where the full energy of the laser beam could be measured) and it is an average approximation from different data sets.
The responsivity of the (*Tx* Energy) monitor changes significantly as function of temperature, therefore a temperature correction must be applied to Equation (1). The temperature correction was derived from the breadboard laser test data and the EM laser TVAC data, where a stable external monitor was present.

$$E(T) = E(T_0) \times (1.0 - 0.0075 \times T + 3.71 \times 10^{-4} \times T^2 - 1.93 \times 10^{-6} \times T^3 - 8.65 \times 10^{-9} \times T^4 \qquad (2)$$

where T_0 is the energy at room temperature (T ~ 24 C). There is no temperature sensor on the SPOT4 detector itself. However, the detector should follow the laser bench temperature and the LEA (with some lag). It does not get as cold as the laser bench temperature or as hot as the LEA electronics.

Note that there was no sub-system TVAC test of the flight transmitter. At system level TVAC there was a fiber-optic pick-off for laser energy measurements which, unfortunately, showed large variations due to fiber optic coupling and transmission changes as a function of temperature and could not used to derive the temperature correction.

4.2 Receiver Energy Calibration

Each LOLA detector has an energy monitor circuit that estimates the received energy (Rx Energy) incident on each detector. The received energy per pulse is a direct measure of the lunar surface reflectivity and is given by:

$$E_{Rx} = E_{Tx} \times \varepsilon_{Rx} \times \frac{A_{Rx} \times \rho}{\pi \times r^2} \qquad (3)$$

where E_{Rx} is the received energy, E_{Tx} is the transmitter energy, ε_{Rx} is the efficiency of the receiver optics (from the telescope to the detector active area), A_{Rx} is the receiver aperture area, ρ is the surface reflectivity and r is the range to the target (lunar surface). By normalizing the received energy to the transmitter energy and knowing the range, the reflectivity of the lunar surface can be estimated.

The energy is essentially a peak sample and hold circuit with an integrator. The energy monitor is after the variable gain amplifier (VGA) and voltage buffer but before the timing circuit so it is affected only by the gain setting but not the threshold. The circuit is

optimized for detection of energies from 0.1 to 3.0 fJ. The energy monitor was characterized at subsystem testing and system level integration.

4.3 Transmitter Calibration

The laser far field pattern was measured at the subsystem (laser) level with a 4-m focal length off-axis parabola collimator and a CCD camera at the focal point. The data were analyzed using commercial beam analysis software (BeamView© by Coherent). The laser beam profiles after the beam expander integration are shown in Fig. 12.

The laser divergence prior to the beam expander integration was:
Laser 1
FF Divergence 1.76 mrad (= 97.8 μrad after ×18 beam expander)
99% energy enclosed within aperture diameter of 5.7 mm - 1.6 X $1/e^2$ dia, or
< 1 % of energy lies outside of 2 x $1/e^2$ diam.
Circularity = 0.91

Laser 2
FF Divergence 1.72 mrad (= 95.6 μrad after ×18 beam expander)
99% energy enclosed within aperture diameter of 5.7 mm - 1.7 X $1/e^2$ dia, or< 1 % of energy lies outside of 2 x $1/e^2$ diam.
Circularity = 0.97

During system level environmental testing the laser far field pattern was measured using an off-axis parabola and a different CCD camera. The data were analyzed using custom-developed software that fit the laser images to a two-dimensional Gaussian surface. Sample of laser images (along with reference cube images and a fiduciary image) are shown in Fig. 13.

The laser far field pattern remained nearly in the fundamental or TEM_{00} mode over the entire operating temperature range. The divergence was calculated as the average of the *x* and *y* Gaussian $1/e^2$ widths. The laser divergence and circularity (defined as the ratio of major to minor axes, in this case, the ratio of the *x* and *y* Gaussian widths obtained by the fit) as a function of temperature are shown in Table 3. (At ambient pressure the transmitter optics is out of focus, which results in high divergence).

4.4 Laser Pointing Jitter

The laser pointing jitter was monitored at the subsystem level and also during the system level environmental testing. Fig. 14 shows the Laser 1 pointing jitter after analyzing 450 images taken under vacuum and at ambient temperature over al temperatures. The images were analyzed for the relative separation between the central laser spot and a reference cube. The jitter in both subsystem and system level environmental testing was approximately 5 μrad in the *x* and *y* directions.

4.6 Laser Wavelength

The laser wavelength at the subsystem delivery was 1064.4 nm. During system level environmental testing the laser wavelength was monitored by a wavemeter (operating in continuous wave – CW -- mode). The overall change in the laser wavelength was ~ 0.1-0.13 nm. Discontinuous changes in the laser wavelength were 0.04 - 0.05 nm. To first order the change in wavelength (without the discontinuous changes) was ~ 0.06-0.07 nm/deg C. The discontinuous changes in the wavelength could be attributed to changes in the mode structure of the laser and/or the wavemeter operation, which will report the wavelength of only one mode.

4.5 Laser Energy

The laser energy at room temperature at the time of subsystem delivery was ~ 2.6 mJ for Laser 1 and ~ 3.0 mJ for Laser 2 after the beam expander. This was verified at the system level prior to laser integration onto the instrument. The laser energy was measured again at the orbiter level (with a different energy meter). The energy for Laser 1 was 2.66 mJ, and 3.22 mJ for Laser 2. The difference between subsystem and system measurements is probably due to the calibration of the energy sensors - the absolute calibration for each meter is 10%. No degradation of the laser energy has been observed from delivery to orbiter integration.

The laser energy varies as a function of temperature. The dependence of the laser energy on the temperature was verified at the subsystem level in air. For Laser 1 the temperature dependence is:

$$E(mJ) = 0.331 + 0.363 \times T - 0.022 \times T^2 + 5.7\times10^{-4} \times T^3 - 5.6\times10^{-6} \times T^4 \qquad (4)$$

and for Laser 2:

$$E(mJ) = 0.359 + 0.397 \times T - 0.021 \times T^2 + 5.0\times10^{-4} \times T^3 - 4.4\times10^{-6} \times T^4 \qquad (5)$$

where T is the laser bench temperature in degrees C. Both lasers exhibited strong hysteresis when the temperature was cycled.

4.7 Laser Pulse Shape and Mode-beating

The laser pulse shape was measured at subsystem (laser) integration using a high-speed photo detector and oscilloscope and during system environmental testing. Sample waveforms from the system level environmental tests are shown in Fig. 12. The pulse width varies from 4.3 to 4.9 ns full width at half maximum (FWHM) amplitude.

The LOLA laser is not a single mode laser. It will occasionally operate in more than one mode and those modes may beat against each other producing a series of very short pulses (shown in Fig. 15 as seen by a high speed photo detector and a fast oscilloscope). The impulse response of the transmit energy monitor will “smear out” the short mode-

beating pulses. However, when the laser mode beats there will be an impact on the time of flight (range) measurement. Laser 1 rarely exhibits multi-mode behavior (1-2 % of the total number of shots in steady state), whereas Laser 2 exhibits multi-mode behavior much more frequently. The multi-mode behavior is also dependent on the laser temperature. The transmit energy monitor can be used to detect the multi-mode behavior of the laser since the peak energy shows a large increase. Thus the *Tx* energy monitor will be used to flag the returns and possibly correct for the distorted laser pulse shapes. For further details of the instrument design and calibration see (Riris and al., 2008).

5. Observation Strategy

In terms of coverage, LOLA under samples the lunar surface and for this reason the basic observational strategy is to operate continuously and obtain as much coverage of the Moon as is possible within operational constraints. Further, the instrument is a nadir-viewing instrument and therefore primarily acquires observations underneath the spacecraft and provides the "landing strip" information described earlier. However, certain exploration and science investigations can require LOLA observations away from the ground track and therefore LOLA is required to operate off-nadir. Off-nadir observations are possible with LOLA and other laser altimeters. Notably, MOLA (Zuber et al., 1992) at Mars and MLA (Cavanaugh et al., 2007) at Mercury, have both obtained off-nadir observations; MOLA on a regular basis as the MGS spacecraft changed attitude to enable the imaging system to acquire specific targets (Smith et al., 2001), and MLA during two flybys in which the emission angle exceeded 60^{o} (Zuber *et al.*, 2008c).

The observation of potential landing sites and special locations, such as inside permanently shadowed regions (where LOLA is one of the few instruments capable of making observations), may require dense observations with coverage as uniform as possible. Off-nadir pointing by only 1 or 2 milliradians from 50-km altitude can move the LOLA swath on the surface by 50 or 100 m and thereby improve the distribution of LOLA tracks across a region.

6. Data Analysis, Interpretation, and Modeling

6.1 LOLA Data

LOLA data packets consist of time-ordered, round-trip, time-of-flight ranges to the lunar surface, preceded by housekeeping and ancillary data. These 3424-byte packets are output over the spacecraft IEEE-1553 data bus at 1-s intervals and aggregated into ~1 megabyte-sized files on the LRO Solid State Recorder. The raw, uncalibrated data comprise the experiment data record product (EDR). After range calibration and orbital processing, the position of each laser spot is located on the surface using a spacecraft trajectory, attitude history, and a lunar orientation model. The reduced data records (RDR) contain calibrated, geolocated pulse returns, altitudes, and reflectivities. Higher-

level gridded and transformed data products are produced from the cumulative RDR product.

The LOLA science data from each downlink tracking pass will be aggregated by the LRO Ground Data System and transmitted daily to the GSFC LOLA Science Operations Center (SOC) computer, together with spacecraft event, housekeeping and attitude data. The raw Deep Space Network (DSN), Universal Space Network (USN), and White Sands 1 (WS1) tracking data and supporting products will also be forwarded to the SOC. Each EDR file, ~300 per day, is processed in a pipeline. The geolocation processing cycle will collect the data records into half-orbits, 25-26 per day, with manageable file sizes (~25 megabyte per product). The northern half-orbit begins at the spacecraft ascending node and the southern half-orbit begins at the descending node, following the LRO Project orbital numbering convention.

The timing of LOLA instrument events is derived from the LRO USO, which is monitored by ground stations. Time systems aboard LRO employ Coordinated Universal Time (UTC) to correlate spacecraft Mission Elapsed Time (MET) to ground time with an accuracy of ±3 ms. The correlation of MET time to Barycentric Dynamical Time (TDB) is maintained at much higher precision by the LR system and orbital theories. The LOLA data analysis uses TDB as its primary time system (see http://tycho.usno.navy.mil/systime.html for details regarding the difference). Spacecraft states relative to the Solar System Barycenter (SSB) at the laser transmit and detector receive times are projected along the instrument boresight and return path vectors to match the observed time-of-flight, correcting for the aberration of light and general-relativistic time delays. SSB states are determined in the Earth Mean Equator of 2000 (J2000) inertial reference frame using lunar spacecraft trajectories and the DE421 planetary ephemeris (Folkner and Williams, 2008). The speed of light c is applied to the boresight time-of-flight to locate the laser bounce point in barycentric coordinates. The bounce points are transformed to a selenodetic coordinate frame about the center of mass of the Moon using the DE421 Moon Mean-Earth and Rotation Pole (MOON_ME) lunar orientation model. The DE421 model incorporates 37 years of Lunar Laser Ranging (LLR) data, thereby providing the geodetic framework for LOLA. The lunar radius and position are then subjected to orbital crossover analysis (Rowlands *et al.*, 1999; Neumann *et al.*, 2001) to minimize the terrain mismatch at the intersections of ground tracks. Empirical adjustment of short-term pointing biases is combined with orbital estimation from tracking data to bring the ground tracks into agreement, and produce a dynamically-consistent, geodetically-precise lunar coordinate framework, as well as an improved lunar potential solution. The crossover adjustment is performed at monthly intervals following the propulsive orbital adjustment maneuvers that break the dynamical orbit solutions.

The cumulative altimetric data are binned and interpolated at appropriate resolution to generate the gridded data record (GDR) products described in the next section. These products are then transformed to Spherical Harmonic Analysis Data Records (SHADR) of shape, time-averaged reflectivity, and related geodetic parameters.

Initial quick-look profiles are generated using orbital and attitude data provided by the GSFC Flight Dynamics Facility, and can be displayed in a web browser. Automated editing flags the noise returns and occasional Earth ranges received by Detector 1. After error checks, labeling, manual inspection of edited products, and registration with images obtained by the co-boresighted LRO cameras (Robinson et al., 2008), the EDR and RDR products are validated for delivery to the Planetary Data System (PDS). Refined altimetry is generated in the course of orbital processing by the GEODYN software system (Pavlis et al., 2001), and is released at quarterly intervals as specified in the LRO-LOLA Data Management and Archive Plan. Releases to the PDS Geosciences Node occur at specific intervals, while the current best solutions are made accessible to LRO scientists via a Data Node of the PDS hosted by the LOLA SOC.

6.2 Quick-look Data Analysis

A quick-look web-based interface has been developed for near-realtime assessment of LOLA data. Data are displayed for each of the five LOLA profiles, and also for the surface reflectivity and roughness. These data are uncorrected and are not suitable for scientific analysis but together with the global map of data distribution can be used for assessing adequacy of coverage and general functioning of the instrument, and in particular for any missing data or changes in the probability of data return from the lunar surface.

7. Science Data Products

Table 4 summarizes expected sizes and production rates for the LOLA Standard Data Products. These products, with detached PDS labels, will be organized into daily and monthly directories. The RDR observations from multiple orbits will be transformed to useful map projections, binned (median-averaged) and interpolated to fill regions lacking data.

A control network for the Moon, consisting of images and control points, will be tied to a topographic reference surface, for which the LOLA GDR is the primary datum. The GDRs are raster Digital Elevation Models of the lunar radius with respect to a spherical datum about the center of mass, and are generated at multiple resolutions (Table 5) as accumulating coverage permits to match the characteristics of image mosaics and other instrument products. Surface slope, roughness, and albedo gridded products will likely be noisier and less amenable to interpolation than altimetry, so will be generated only at a subset of resolutions given in Table 5 unless a specific need arises, in which case Special Products will be produced. The size of the products at highest resolution may require that they be aggregated in subsets of global coverage. Global products use the equi-rectangular map projection, while the higher-resolution products afforded by dense polar coverage use the Polar Stereographic projection. Tiling will be employed to limit the size of individual products to less than 2 GB to facilitate electronic data transfer. The GDRs are formatted as binary images. Binary elevation data may consist of 16-bit integers scaled to a dynamic range of 1728 to 1748 km, or as 32-bit integers scaled to millimeters.

The resolution of equi-rectangular pixels will be powers of two pixels per degree of longitude and latitude. The resolution of polar projected pixels will be integral numbers of meters, scaled by a radius of 1737.4 km. Anticipated tiles are shown in Fig. 16. Where feasible, products may also be provided in a geo-referenced JPEG-2000 format.

8. Summary

The LOLA instrument was delivered to the LRO spacecraft in April 2008 and along with the other instruments integrated with the spacecraft. As of January 2009, the LRO spacecraft has completed thermal vacuum testing and is being readied for shipment to the launch site. The LOLA instrument is a significant advance in capability over previous planetary laser altimeters with its multiple beams and laser ranging component, and is expected to contribute a unique dataset for lunar science and exploration.

9. Acknowledgements

We are pleased to acknowledge the support and assistance of the LRO Project, particularly the Payload Manager, Arlin Bartels, and the Project Manager Craig Tooley, without whom the LOLA instrument could not have been built. We also thank the Review Boards that provided sanity and constructive thought during the LOLA development process.

References

Abshire, J. B.*, et al.*: 2005, Geoscience Laser Altimeter System (GLAS) in the ICESat mission: On-orbit measurement performance, *Geophys. Res. Lett.* **43**, L21S02.

Araki, H., Tazawa, S., Noda, H., Tsubokawa, T., Kawano, N., and Sasaki, S.: 2007, Topographic exploration of the Moon by laser altimeter onboard SELENE (LALT), *Geophys. Res. Abstracts* **9**.

Cavanaugh, J. F.*, et al.*: 2007, The Mercury Laser Altimeter instrument for the MESSENGER mission, *Space Sci. Rev.* **131**, 451-480.

Chin, G.*, et al.*: 2007, Lunar Reconnaissance Orbiter overview: The instrument suite and mission, *Space Sci. Rev.*

Cook, A. C., Watters, T. R., Robinson, M. S., Spudis, P. D., and Bussey, D. B. J.: 2000, Lunar polar topography derived from Clementine stereoimages, *J. Geophys. Res.* **105**, doi: 10.1029/1999JE001083.

Dickey, J. O.*, et al.*: 1994, Lunar laser ranging: A continuing legacy of the Apollo program, *Science* **265**, 482-490.

Folkner, W. M., and Williams, J. G.: 2008, Planetary Ephemeris DE421 for Phoenix Navitation, Jet Propulsion Laboratory, Pasadena, CA.

Frey, H., Shockey, K. M., Frey, E. L., Roark, J. H., and Sakimoto, S. E. H.: 2002, Ancient lowlands on Mars, *Geophys. Res. Lett.* **29**, 10.1029/2001GL013832.

Goossens, S., and Matsumoto, K.: 2008, Lunar degree 2 potential Love number determination from satellite tracking data, *Geophys. Res. Lett.* **35**, doi:10.1029/2007GL031960.

Kamalakar, J. A.*, et al.*: 2005, Lunar ranging instrument for Chandrayaan-1, *J. Earth Syste. Sci.* **114**, 725-731.

Konopliv, A. S., Asmar, S. W., Carranza, E., Sjogren, W. L., and Yuan, D.-N.: 2001, Recent gravity models as a result of the Lunar Prospector mission, *Icarus* **150**, 1-18.

Neumann, G. A., Rowlands, D. D., Lemoine, F. G., Smith, D. E., and Zuber, M. T.: 2001, The crossover analysis of MOLA altimetric data, *J. Geophys. Res.* **106**, 23,753-23,768.

Nozette, S.*, et al.*: 1994, The Clementine mission to the Moon: Scientific overview, *Science* **266**, 1835-1839.

Pavlis, D. E., Poulouse, S. G., Rowton, S. C., and McCarthy, J. J.: 2001, GEODYN Operations Manuals, Raytheon ITTS Contractor Report, Lanham, MD.

Qian, H., *et al.*: 2008, Topography of the Moon from the Chang'e Laser Altimetry Data.

Ramos-Izquierdo, L., et al.: 2009, The Lunar Orbiter Laser Altimeter (LOLA) optical subsystem.

Riris, H., *et al.*: 2008, LOLA Calibration Report, NASA/Goddard Space Flight Center, Greenbelt, MD.

Robinson, M. S.*, et al.*: 2008, The Lunar Reconnaissance Orbiter Camera (LROC), *Space Sci. Rev.*

Rowlands, D. D., Pavlis, D. E., Lemoine, F. G., Neumann, G. A., and Luthcke, S. B.: 1999, The use of laser altimetry in the orbit and attitude determination of Mars Global Surveyor, *Geophys. Res. Lett.* **26**, 1191-1194.

Schultz, R. A., Okubo, C. H., Goudy, C. L., and Wilkins, S. J.: 2004, Igneous dikes on Mars revealed by Mars Orbiter Laser Altimeter topography, *Geol. Soc. Am. Bull.* **32**, 889-892.
Schutz, B. E.: 2001, Laser altimetry and lidea from ICESat/GLAS, *IEEE Geoscience and Remote Sensing* **3**, 1016-1019.
Smith, D. E., Zuber, M. T., Neumann, G. A., and Lemoine, F. G.: 1997, Topography of the Moon from the Clementine LIDAR, *J. Geophys. Res.* **102**, 1591-1611.
Smith, D. E.*, et al.*: 1999, The global topography of Mars and implications for surface evolution, *Science* **284**, 1495-1503.
Smith, D. E.*, et al.*: 2001, Mars Orbiter Laser Altimeter: Experiment summary after the first year of global mapping of Mars, *J. Geophys. Res.* **106**, 23689-23722.
Sun, X., Abshire, J. B., Neumann, G. A., and Zuber, M. T.: 2001, Radiometry measurements of Mars at 1064 nm using the Mars Orbiter Laser Altimeter, *EOS Trans. Am. Geophys. Un.* **82**.
U.S. Geological Survey.: 2002.Color-coded topography and shaded relief map of the lunar near side and far side hemispheres, Flagstaff, AZ.
Wieczorek, M. A.: 2007, Gravity and topography of the terrestrial planets, *Treatise on Geophysics* **10**, 165-206.
Zuber, M. T., Smith, D. E., Lemoine, F. G., and Neumann, G. A.: 1994, The shape and internal structure of the Moon from the Clementine mission, *Science* **266**, 1839-1843.
Zuber, M. T., Smith, D. E., Alkalai, L., Lehman, D. H., M.M., W., and Team, G.: 2008a, Outstanding questions on the internal structure and thermal evolution of the Moon and future prospects from the GRAIL mission, *Lunar Planet. Sci. Conf.* **XXXIX**, #1074.
Zuber, M. T.*, et al.*: 1992, The Mars Observer Laser Altimeter investigation, *J. Geophys. Res.* **97**, 7781-7797.
Zuber, M. T.*, et al.*: 2008b, The Lunar Reconnaissance Orbiter laser ranging investigation, *Space Sci. Rev.*
Zuber, M. T.*, et al.*: 2008c, Laser altimeter observations from MESSENGER's first Mercury flyby, *Science* **321**, 77-79.

Figure Captions

Fig. 1 Clementine lunar topography (Smith et al., 1997).

Fig. 2 LOLA's five laser spot pattern.

Fig. 3 Surface slope measurements possible from LOLA profiles.

Fig. 4 *(a) Example of south polar coverage, lat 88^{o}S to the pole. (b) Example of coverage lat 80S (or N) to the pole* ***fix figure and caption.***

Fig. 5 LOLA instrument configuration.

Fig. 6 LOLA functional block diagram.

Fig. 7 Laser transmitter showing two lasers.

Fig. 8 Receiver and fiber bundle.

Fig. 9 Aft optics and test port.

Fig. 10 Detector thresholds.

Fig. 11 Pulse energy calibration.

Fig 12 Laser transmitter profiles showing transmit pulse shape.

Fig. 13 Laser far field.

Fig. 14 Spatial pattern of pulse energy.

Fig. 15 Laser mode beating.

Fig. 16 Equirectangular map projection. Lines show tiling subdivisions of LDEM_256 (bold), LDEM_512 (fine), and LDEM_1024 (dashed).

.

Table 1 Assumptions in LOLA Instrument Investigation

Lander scale	~5 m	Approx. size of Apollo module
Landing area	~50 to 100 m	????
Slope accuracy in 2 directions	$\pm 1^{o}$, 10m baseline	
Elevation precision	±0.1 m	
Radial accuracy	<1 m	Includes orbit and instrumental errors
Horizontal accuracy	<50 m	Landing site size.
Surface roughness	0.3 m	Typical height clearance of Mars lander
Spacecraft position	H: 50 m; V: <1 m	Landing site positional knowledge
Spacecraft timing	3 ms	Spacecraft velocity is ~1.6 m/s

Table 2 Key Instrument Parameters

Parameter	**Value**
Laser Wavelength	1064.4 nm
Pulse Energy	2.7/3.2 mJ (laser1/laser2)
Pulse Width	~ 5 ns
Pulse Rate	28 ± 0.1 Hz
Beam Divergence	100 ± 10 µrad
Beam Separation	500 ± 20 µrad
Receiver Aperture Diameter	0.14 m
Receiver Field of View	400 ± 20 µrad
Receiver Bandpass Filter	0.8 nm
Detector responsivity (nominal)	300 kV/W
Detector active area diameter	0.7 mm
Detector electrical bandwidth	46 ± 5 MHz
Timing Resolution	0.5 ns

Table 3 Laser Output Beam Properties

	Laser 1 (μrad)	Circularity	Laser 2 (μrad)	Circularity
Ambient 1 Atm	153.1	Out of focus	147.9	Out of focus
Ambient 0 ATM (Start)	100.0	1.08	94. 9	1.19
Hot Qual.	106.7	0.96	97. 5	1.18
Cold Qual./Op.	103.6	1.30	110.7	1.24
Hot Operational	104. 5	1.29	102.5	1.17
Ambient 0 Atm (End)	109.9	1.14	101.7	1.30

Table 4 Standard Data Product Sizes and Delivery Rates

Product	**Product Size**	**Production Rate**	**Expected Number of Products for Nominal Mission**	**Expected Total Data Volume for Nominal Mission**
LOLA_EDR	1 MByte	296 per day**,** average	108000	108 GB
LOLA_RDR	24 MByte	25-26 per day	9400	225 GB
LOLA_GDR	~2 GByte	monthly refinements of ~100 data products	100	200 GB
LOLA SHADR	5 MByte	release at quarterly intervals	4	~1 GB

Table 5 LOLA equi-rectangular Map-projected Digital Elevation Models

Product	Product Size	Pixel size (m in lat)	Number/size of tiles	Bits per pixel
LDEM_4	4 MByte	7580.8	Global, 0-360	32
LDEM_16	64 MByte	1895	Global, 0-360	32
LDEM_32	256MByte	947.6	Global, 0-360	32
LDEM_64	1 GByte	473.8	Global, 0-360	32
LDEM_128	2 GByte	236.9	Global, 0-360	16
LDEM_256	4x2GB	118.45	4 tiles, longitudes 0:180:360 by N/S	16
LDEM_512	16x2GB	59.225	16 tiles, longitudes 0:45:90:135:180:225:270:315:360 by N/S	16
LDEM_1024	64x2GB	29.612	64 tiles, longitudes as above, in 22.5° latitude bands	16

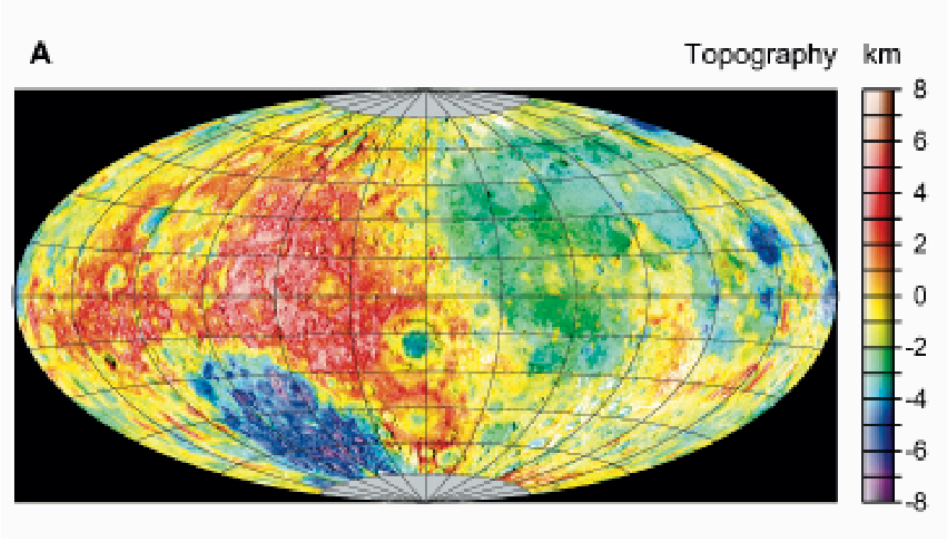

Smith et al.
Figure 1

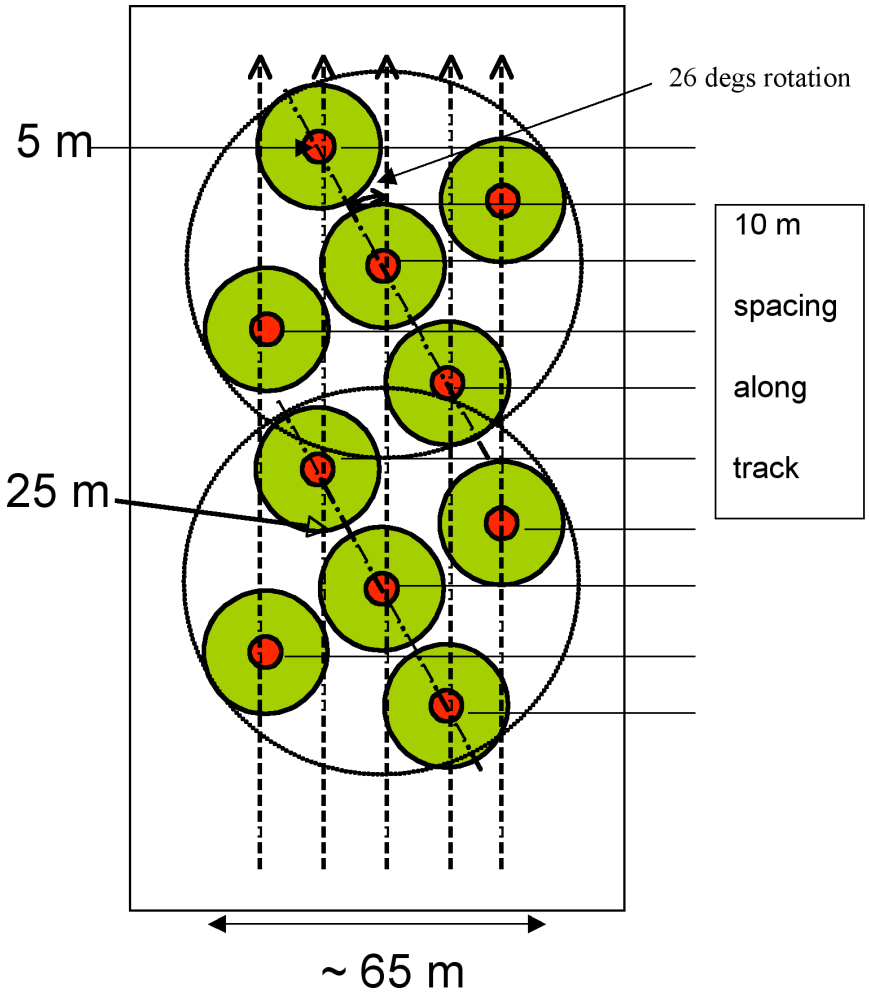

Smith et al.
Figure 2

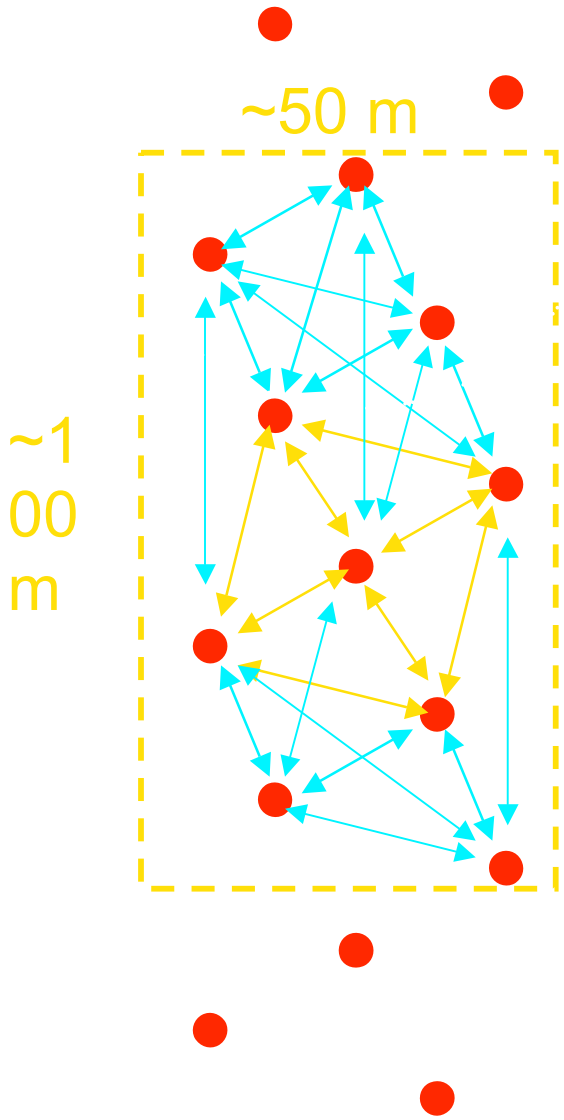

Smith et al.
Figure 3

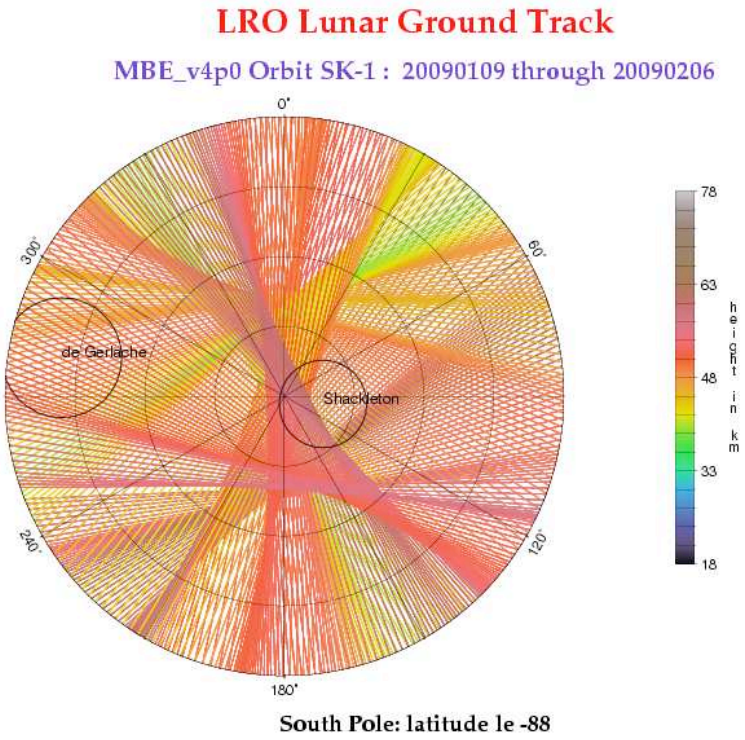

Smith et al.
Figure 4a

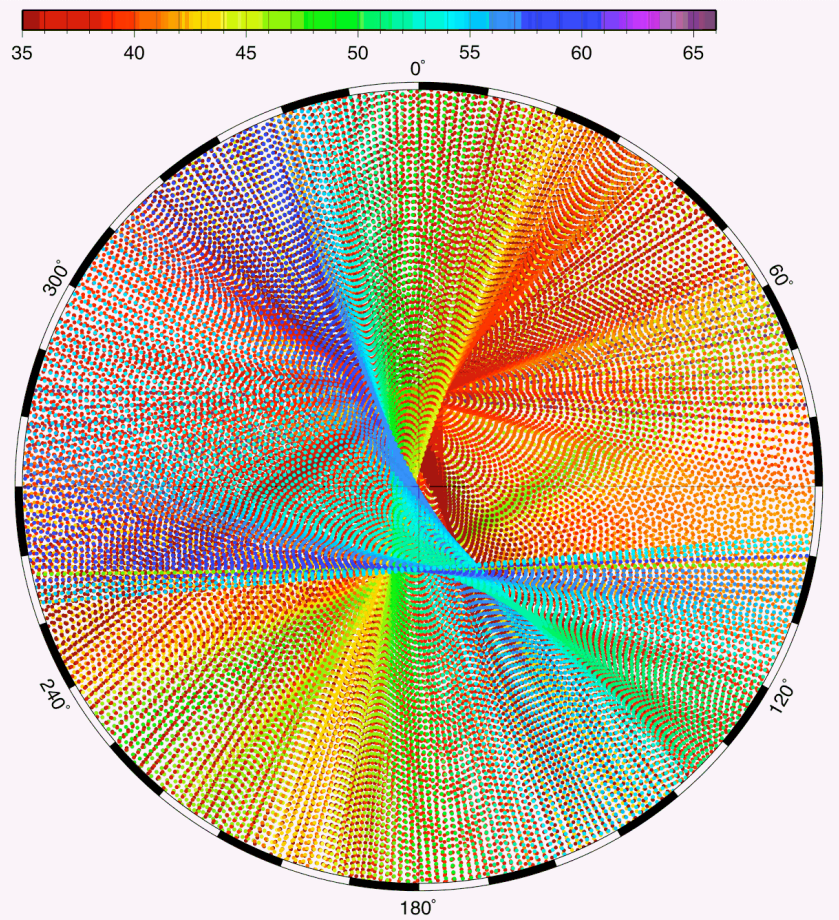

Smith et al.
Figure 4b

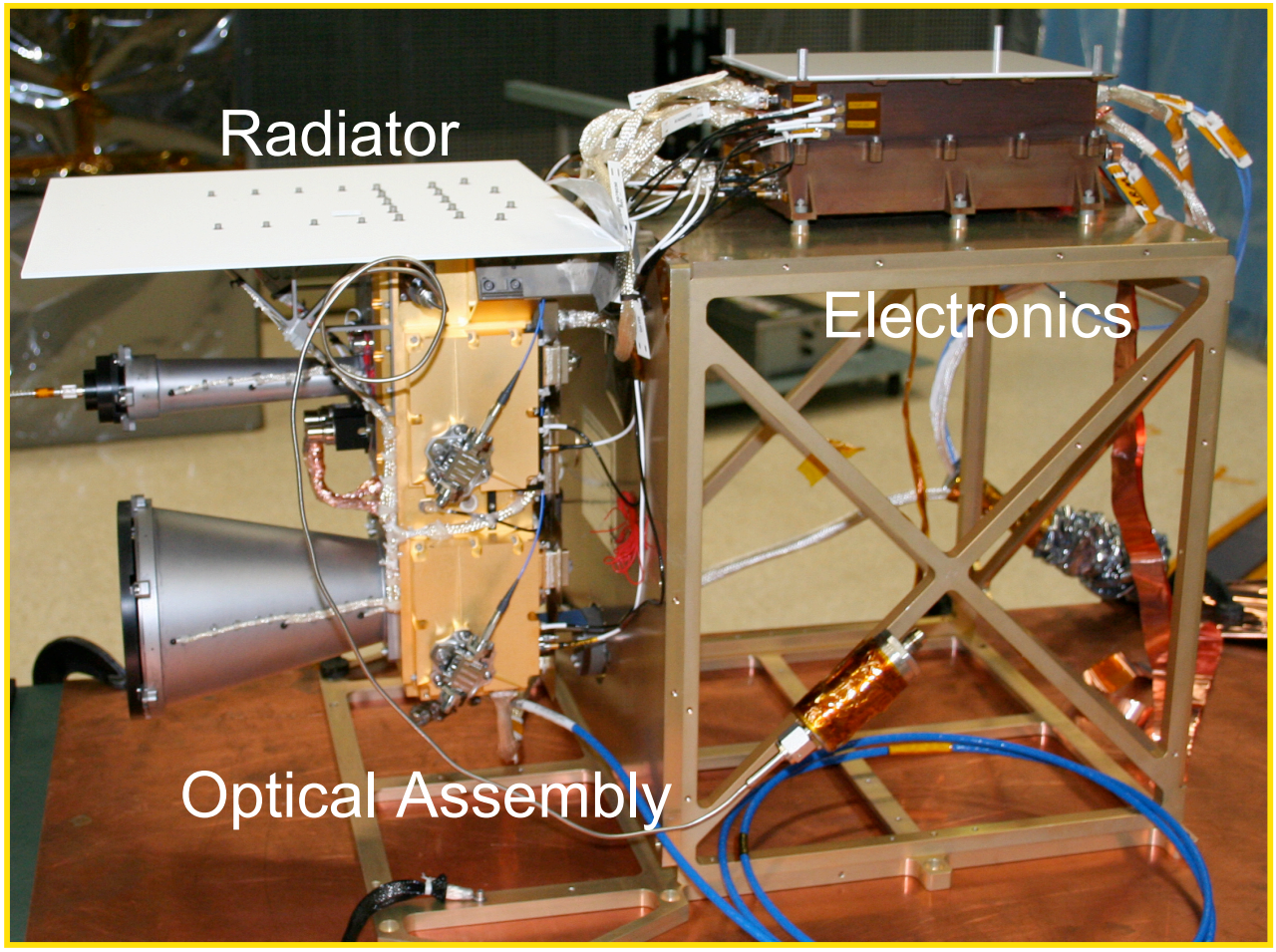

Smith et al.
Figure 5

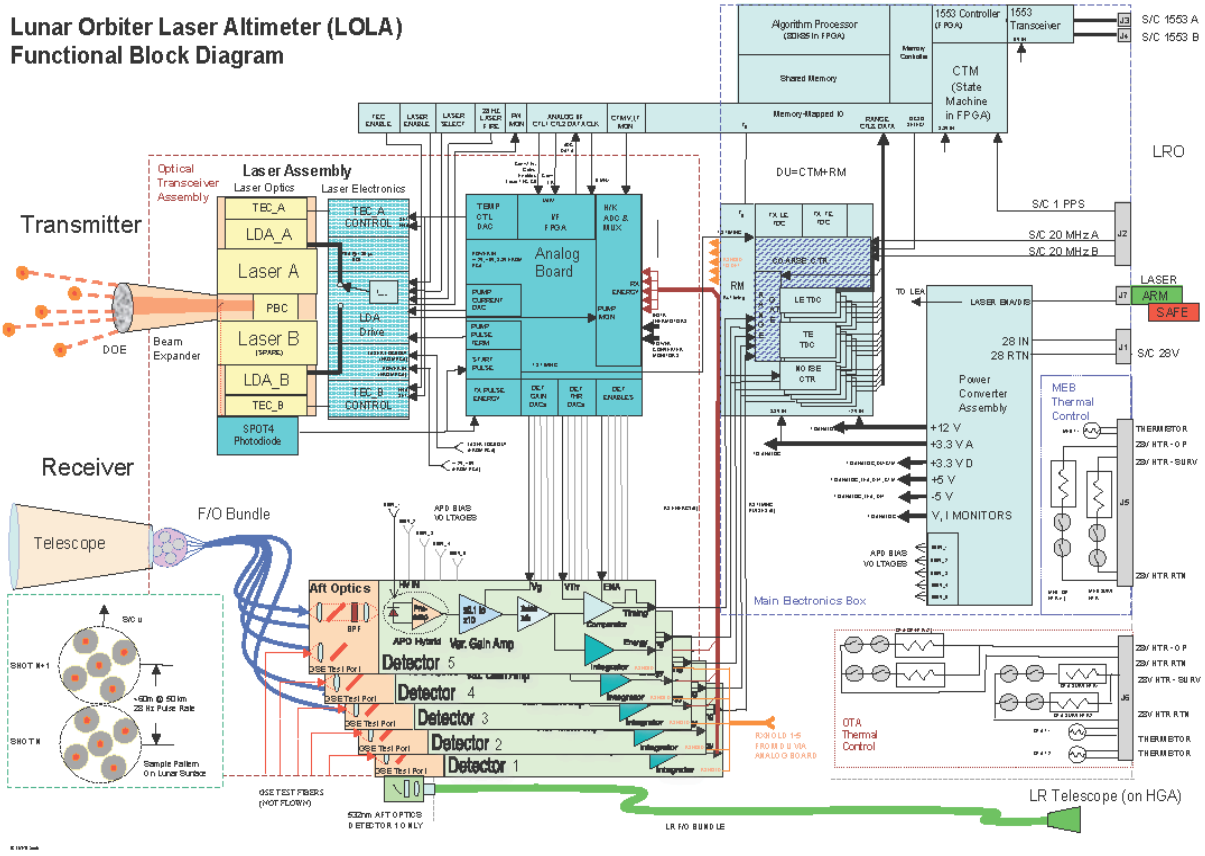

Smith et al.
Figure 6

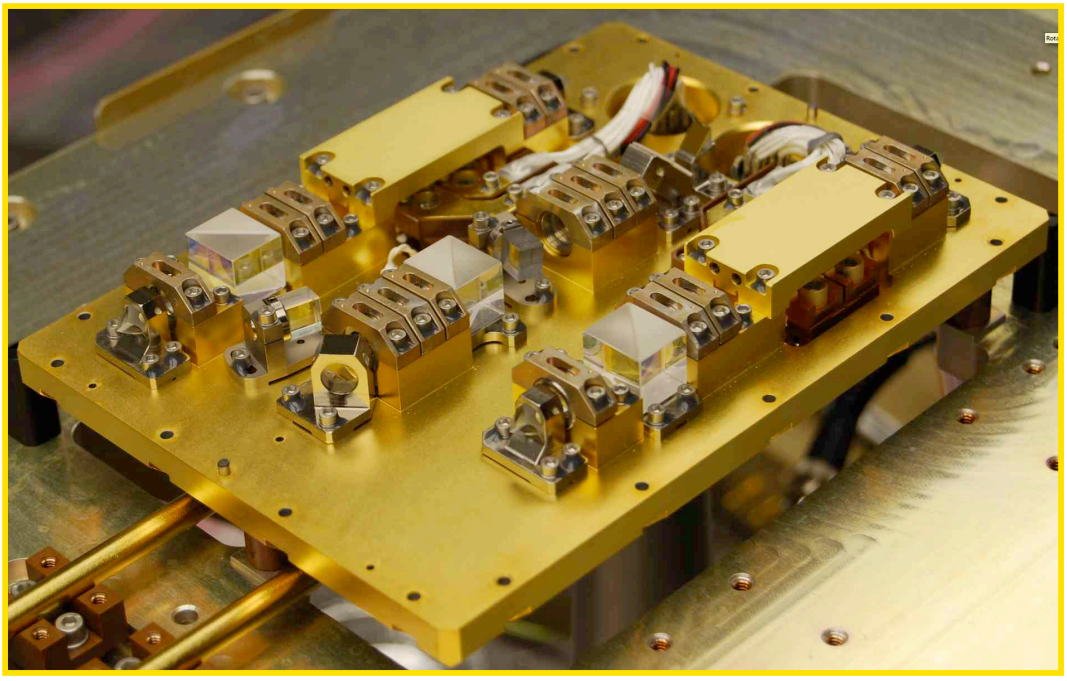

Smith et al.
Figure 7

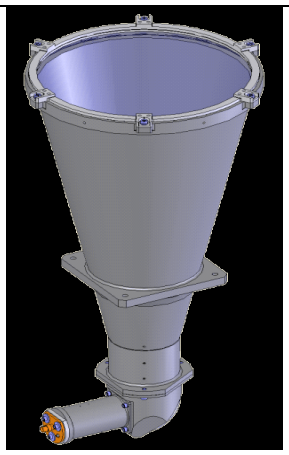

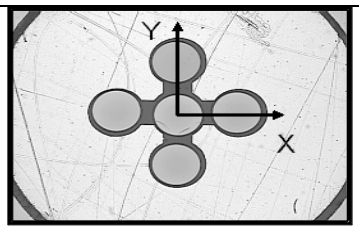

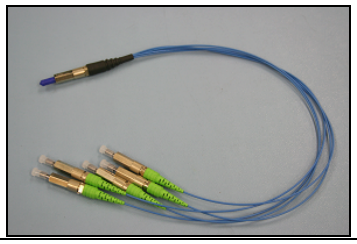

Smith et al.
Figure 8

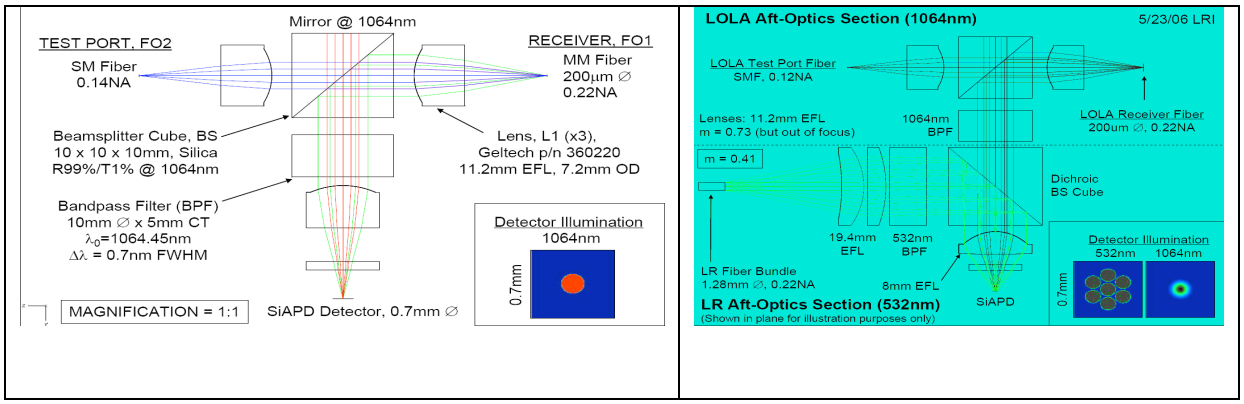

Smith et al.
Figure 9

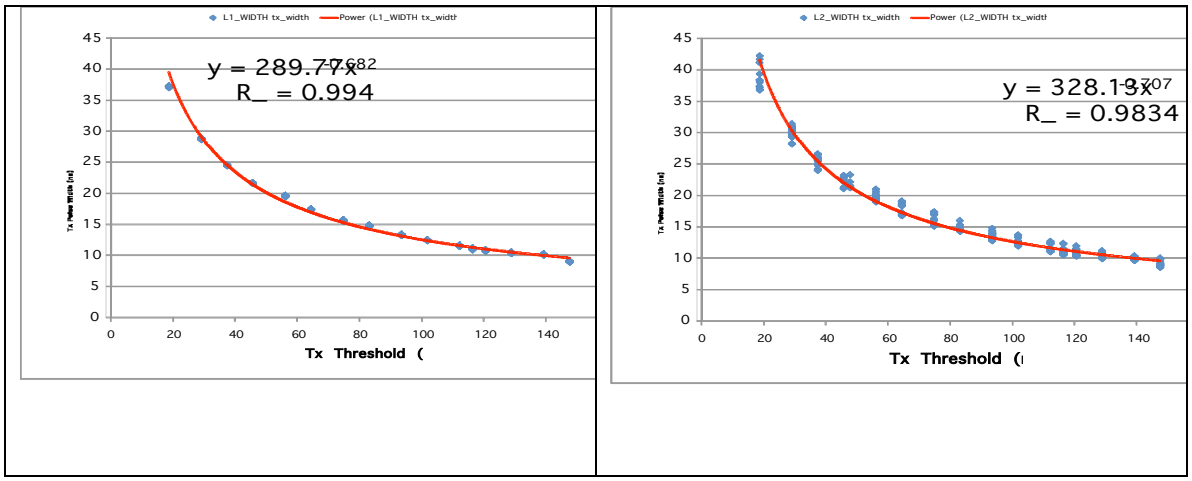

Smith et al.
Figure 10

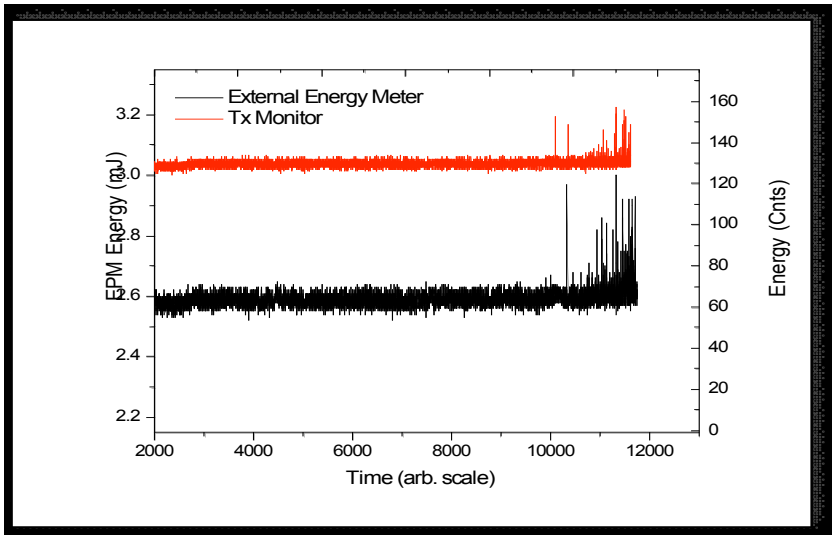

Smith et al.
Figure 11

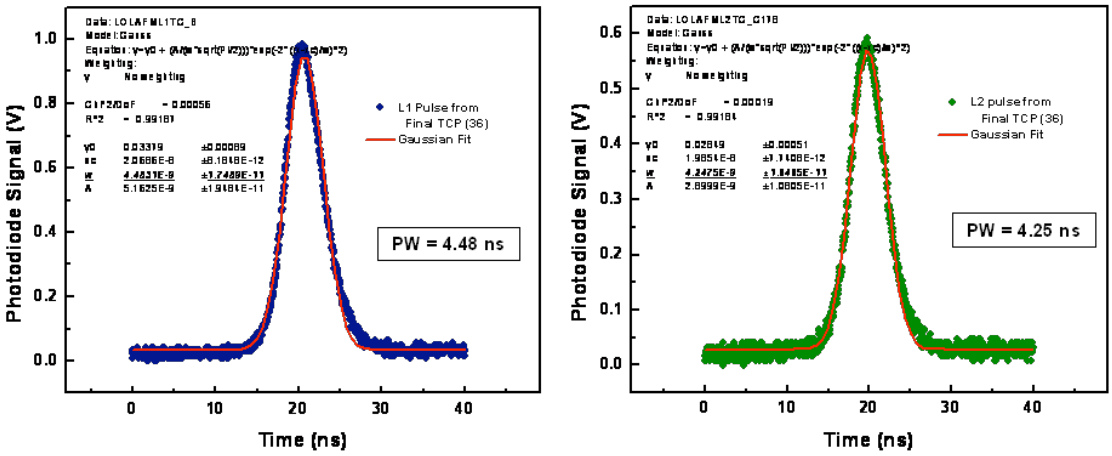

Zuber et al.
Figure 12

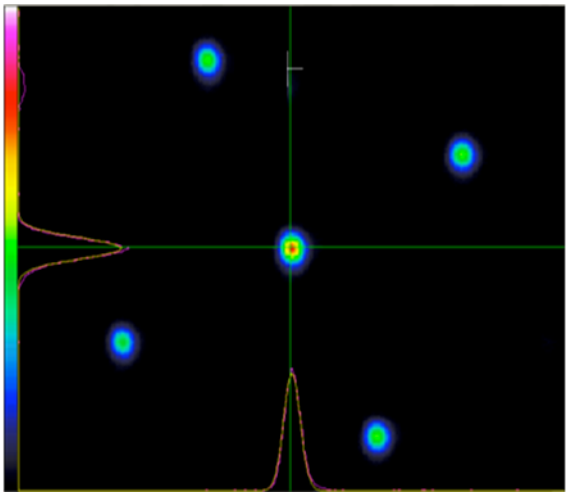	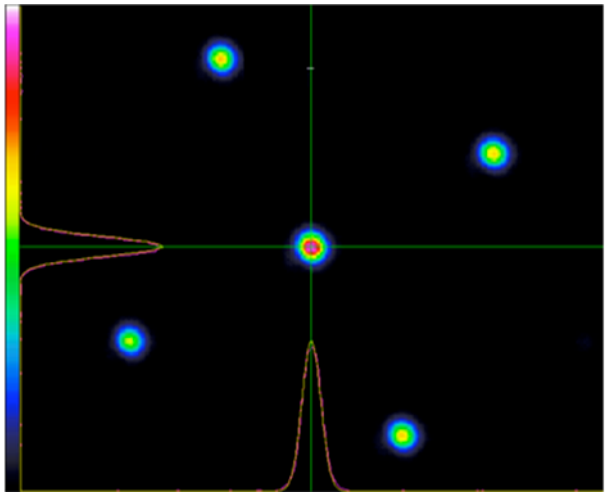
Laser 1 profile with CCD at simulated vacuum Focus (18 mm from OAP focal plane)	Laser 2 profile with CCD at simulated vacuum Focus (18 mm from OAP focal plane)

Smith et al.
Figure 13

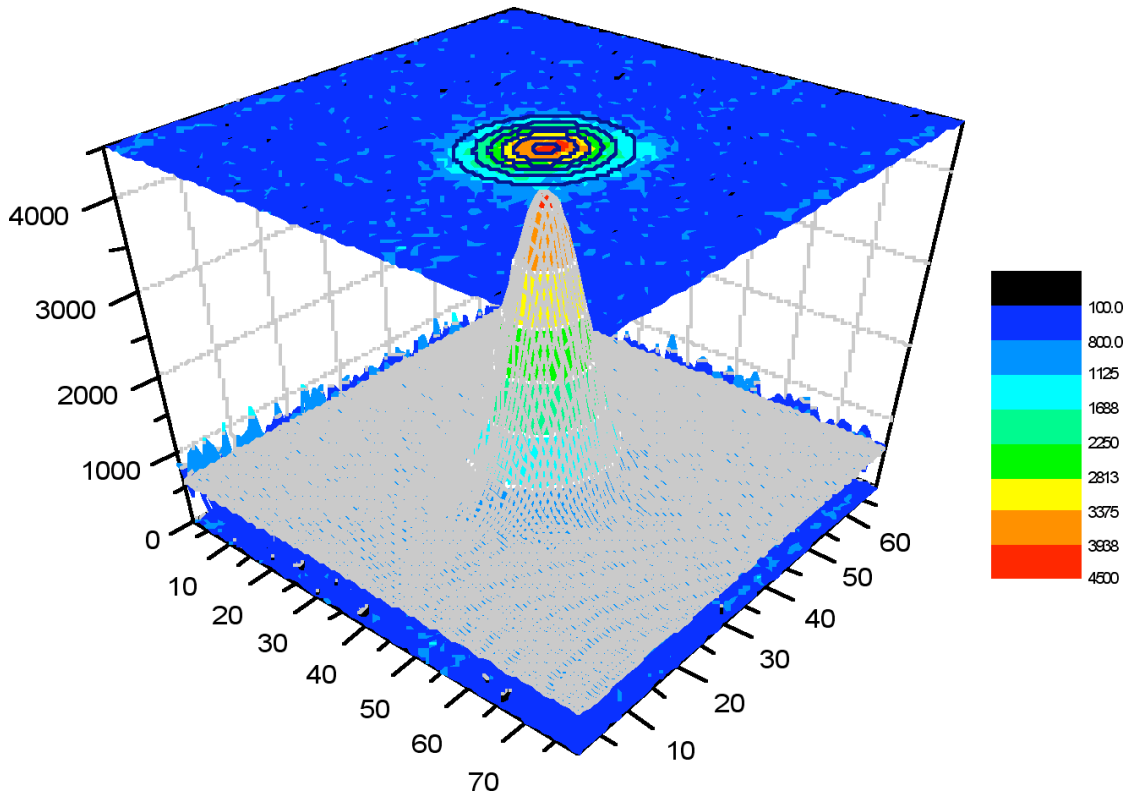

Smith et al.
Figure 14

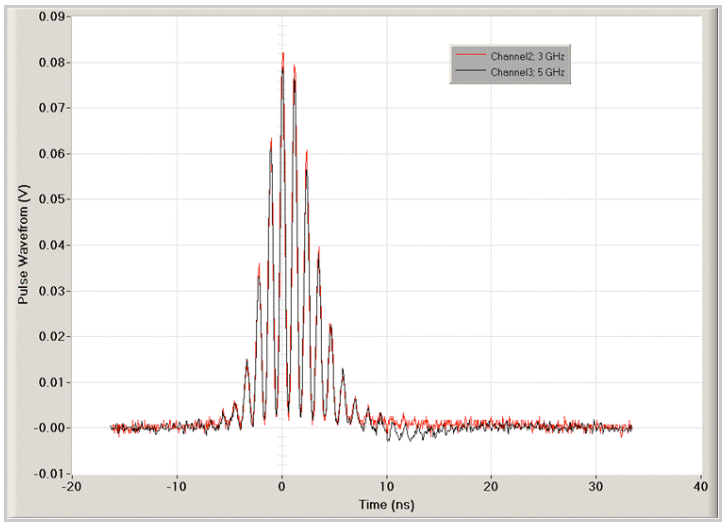

Smith et al.
Figure 15

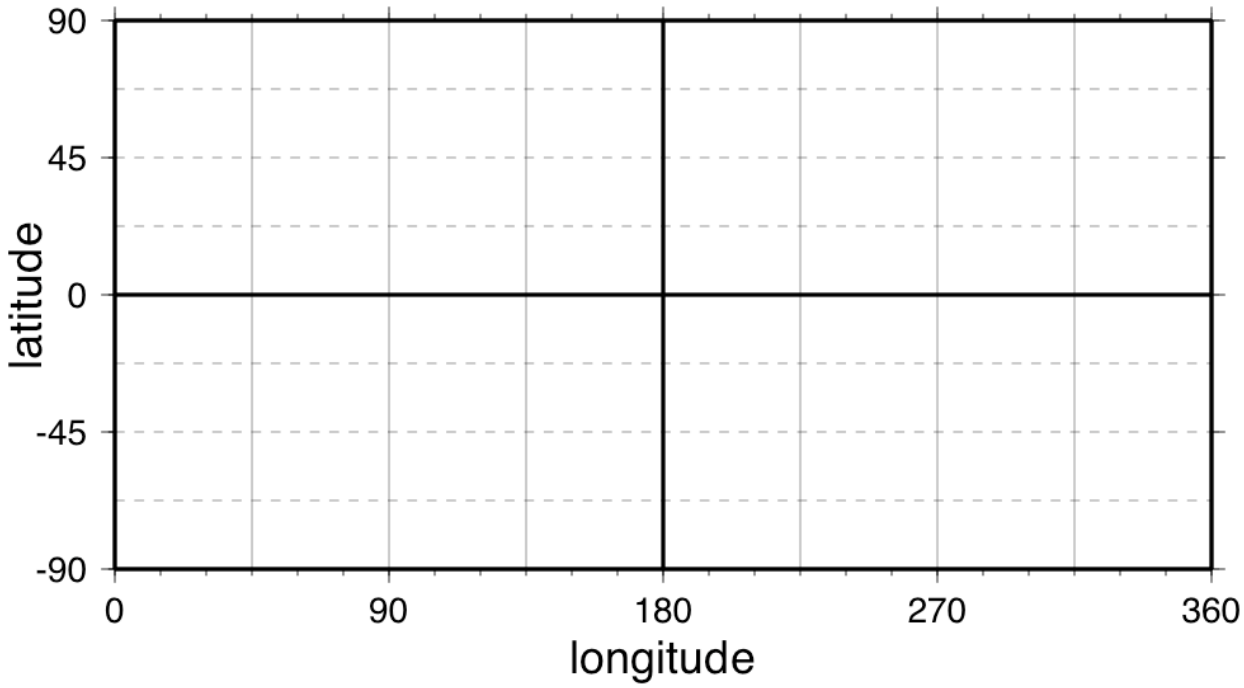

Smith et al.
Figure 16